This article has been accepted for publication in IEEE Transactions on Instrumentation and Measurement. This is the author's version which has not been fully edited and content may change prior to final publication. Citation information: DOI 10.1109/TIM.2025.3568966

Generative Models Training based on FEM Simulations towards improved Defect Detection

Anastasios Tzelepakis, Nikolaos Dimitriou, *Member, IEEE*, Paschalis Charalampous, Konstantinos Tsongas, Dimitrios Tzetzis and Dimitrios Tzovaras, *Senior Member, IEEE*

***Abstract*—Defect prediction and quality control are critical in manufacturing, where Convolutional Neural Networks (CNNs) demonstrate significant potential. However, traditional Finite Element Method (FEM) simulations, despite their accuracy, are hindered by high computational demands. This paper introduces a novel framework that integrates FEM simulations with generative CNNs to predict strain distributions during antenna manufacturing. By employing physics-informed dataset generation from FEM simulations, the proposed method trains a generative CNN to predict strain distributions during antenna manufacturing, enabling physically consistent strain predictions. Validated against FEM-calculated data, the framework demonstrates its efficacy in defect prevention, while addressing the limitations of traditional offline FEM capabilities. Furthermore, a comprehensive analysis of weight initialization and cost function choices, along with experimental validation, highlights the method's efficiency, establishing a cost-effective and practical approach to integrating numerical simulations with CNN-based deep learning in manufacturing.**

***Index Terms*—Defect prediction, finite element method, generative AI, simulation, physics-informed dataset generation.**

I. Introduction

In the context of antenna manufacturing, a critical issue arises during the bending process, where the antenna is placed on the bending surface using a robotic arm, as seen in Fig. 1. There are cases where the robotic arm does not place the antenna accurately, resulting in misplacements characterized by offsets on the X-axis, Y-axis, or rotations in the XY-plane. These misplacements have significant implications, as the pneumatic press used for bending may induce unintended strain distributions, leading to defects such as cracks and alterations in mechanical properties. Hereupon, a Finite Element (FE) model was created to replicate the effects of the misplacement, as well as to determine the developed strain, and deformation that potentially could be provoked. These numerical simulations confirmed the hypothesis that misplacing the antenna can indeed cause defects, as observed during a thorough inspection of the production line [1].

Deep Learning (DL) has revolutionized manufacturing, significantly advancing defect detection [2], [3], [4], [5], failure prediction [6], and quality control processes [7], aligning with the goals of Zero Defect Manufacturing. Among these, Convolutional Neural Networks (CNNs) have become indispensable for their ability to analyze large datasets and extract complex patterns, enabling precise anomaly detection and process optimization. These capabilities have been applied in tasks such as visual inspection, surface defect detection, and predictive maintenance, driving cost savings and improved product quality.

The Finite Element Method (FEM) has long been a cornerstone for numerical simulations, offering unparalleled accuracy in analyzing structural integrity, thermal performance, and material behavior under various conditions [8]. In manufacturing processes like bending, FEM excels at predicting strain distribution and deformation, optimizing material efficiency and minimizing defects. However, FEM's widespread industrial adoption is limited by its high computational cost and time inefficiency, particularly for real-time applications.

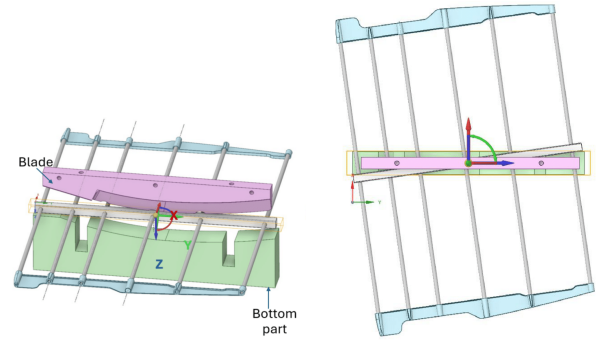

f

Fig. 1. (a) Antenna placement on the bending surface during the manufacturing process, with the blade and bottom part labeled. (b) Top view illustrating an imprecise placement with 0 mm offsets on the x-axis and y-axis, and a 5-degree rotation in the XY-plane.

This paper addresses these limitations by integrating FEM simulations with generative AI to predict strain fields during antenna bending processes. By employing CNNs trained via physics-informed dataset generation, the proposed framework

Manuscript received Month xx, 2xxx; revised Month xx, xxxx; accepted Month x, xxxx. This work was supported by the European Commission through the H2020 programme under grant OPTIMAI "Optimizing Manufacturing Processes through Artificial Intelligence and Virtualization" (ID: 958264), and through the Horizon Europe programme under grant ENCIRCLE "Enabling Circular Value Chains via Production Digitization and Human Empowerment" (ID:101178230). The publication of the article in OA mode was financially supported by HEAL-Link.

Anastasios Tzelepakis, Nikolaos Dimitriou, Paschalis Charalampous and Dimitrios Tzovaras are with the Information Technologies Institute, Centre for Research and Technology Hellas, Thessaloniki, 57001, Greece (e-mail: anastzel@iti.gr; nikdim@iti.gr; pcharalampous@iti.gr; dimitrios.tzovaras@iti.gr).

Konstantinos Tsongas is with the Industrial Engineering and Management Department, International Hellenic University, Thessaloniki, 57001, Greece (e-mail: k.tsongas@ihu.edu.gr).

Konstantinos Tsongas and Dimitrios Tzetzis are with the Digital Manufacturing and Materials Characterization Laboratory, School of Science and Technology, International Hellenic University, Thessaloniki, 57001, Greece (e-mail: k.tsongas@ihu.edu.gr; d.tzetzis@ihu.edu.gr).

This work is licensed under a Creative Commons Attribution-NonCommercial-NoDerivatives 4.0 License.
For more information, see https://creativecommons.org/licenses/by-nc-nd/4.0/

This article has been accepted for publication in IEEE Transactions on Instrumentation and Measurement. This is the author's version which has not been fully edited and content may change prior to final publication. Citation information: DOI 10.1109/TIM.2025.3568966

delivers physically consistent predictions, mitigating defects caused by manufacturing inaccuracies. This approach bridges the gap between FEM precision and the efficiency of AI, offering a practical solution for defect prediction in antenna manufacturing. Here, defect prediction refers to predicting strain fields that exceed material limits and would cause cracks or fractures if the bending process proceeds unmodified. The main contributions are as follows.

1) FEA-AI Integration: Introducing a hybrid framework that combines FEM simulations and CNN-based generative models to enhance predictive accuracy in critical manufacturing processes like bending.
2) Optimized CNN Design: Investigating the impact of weight initialization and loss function choices on CNN-based image synthesis, ensuring fast, accurate and physically consistent predictions.
3) Physics-Informed Dataset Generation: Leveraging FEM-generated datasets to train the CNN, enabling efficient real-time prediction of strain fields and structural integrity.
4) Practical Demonstration: Validating the method's applicability by demonstrating its ability to predict antenna defects based on misplacement in the bending process.

The rest of the paper is structured as follows: Section II provides a review of related work in the domains of DL and FEA for defect prediction tasks in industrial applications. In Section III, the specific use case of defect prediction examined in this study, along with the proposed methodology is outlined. This section also includes a detailed description of the available data and introduces the utilized deep architecture. Section IV presents the evaluation of the methodology and showcases the experimental results. Finally, Section V offers concluding remarks to summarize the findings of this study.

II. Related Work

In this section, an overview of the most recent work related to the proposed method is provided. Since a DL model is developed to generate images akin to the ones produced utilizing FEM simulations; an elaboration on the recent advancements in the fields of defect prediction via DL, FEM simulations, and generative AI is conducted.

A. Defect Prediction via Deep Learning and Generative AI

The integration of Machine Learning (ML) approaches in Industry 4.0 has transformed manufacturing operations, creating smart factories that use sensors and devices to continuously collect data. ML algorithms analyze this data to improve efficiency and quality without major resource changes.In specific, ML's predictive capabilities enable intelligent decision support systems for various manufacturing tasks, including inspection, maintenance, quality improvement, optimization, and scheduling [9]. Moreover, ML techniques have significantly advanced defect detection, particularly through computer vision technology based on CNN [10]. As an emerging representative of AI, DL is already considered a mainstream technology for industrial vision [11], providing researchers with a reference and guidance for applying advanced ML technology effectively. Finally, the work in [12] introduced a real-time quality control solution applied in antenna manufacturing, leveraging lightweight Deep Residual Networks and Blockchain technology to enhance defect detection efficiency and maintain low inference times

It should be noted that ML has become a powerful tool for image synthesis, producing realistic, high-quality images. Recently, generative models like Generative Adversarial Networks (GANs) and Variational Autoencoders (VAEs) have transformed image synthesis by learning complex patterns from large datasets. DL techniques, especially CNNs, need large annotated datasets for supervised learning. Hence, to address this issue, a novel data augmentation framework deploying GAN technologies was introduced in order to create synthetic images [13]. In general, automated defect inspection modules in manufacturing industries often faces a shortage of defect samples. Therefore, defect-GAN methodologies were introduced to generate realistic and diverse defect samples for training inspection networks [14]. The author in [15] explored the capability to predict future events in industrial processes to improve manufacturing and prevent defects. The study introduced a method employing 3D Convolutional Neural Networks (3DCNN) to model changes in the 3D shape of objects based on past measurements.

B. Defect Prediction using Finite Element Method simulations

FEM is one of the efficient numerical approaches simulating complex industrial processes and optimizing structural integrity, aiding in defect prediction and prevention. In [16], the authors introduced a novel generalized Lagrangian formulation to analyze industrial forming procedures, where the suggested methodology can be applied in various types of analysis for both fluid and solid environments. FEA has been essential for optimizing the design and structural integrity of pneumatic press machines [17] and crucial for chipless manufacturing processes like cold stamping. In [17], FEA played a vital role in designing, analyzing, and optimizing the machine's structural components. Furthermore, advancements in FEA have led to significant progress in understanding and optimizing severe plastic deformation (SPD) methods like semi-constrained groove pressing (SCGP) [18]. In SCGP, researchers induced repetitive shear deformation in commercially pure aluminium plates using asymmetrically grooved dies. Moreover, the paper in [19] presented an improved looping method for generating quadrilateral finite elements, customized for automated metal forming simulations. This method incorporates a novel splitting criterion, an artificial boundary scheme, and an optimal nodal placement scheme, all designed to enhance mesh quality for metal forming engineering applications.

It is worth mentioning that the past ten years ML techniques are being increasingly integrated into numerical simulation processes to improve accuracy, efficiency, and predictive capabilities across diverse domains. The work in [20] focuses on predicting failure pressure in high-strength pipes with stray current corrosion defects, and a novel approach was introduced, that combines parametric FE modeling with multilayer feed-forward Artificial Neural Networks (ANN). Combining

This work is licensed under a Creative Commons Attribution-NonCommercial-NoDerivatives 4.0 License.
For more information, see https://creativecommons.org/licenses/by-nc-nd/4.0/

This article has been accepted for publication in IEEE Transactions on Instrumentation and Measurement. This is the author's version which has not been fully edited and content may change prior to final publication. Citation information: DOI 10.1109/TIM.2025.3568966

causal relationships with hidden dependencies from large datasets, hybrid modeling enables the development of comprehensive systems [21]. The application of ML and numerical methodologies in predicting structural behavior and optimizing manufacturing processes is evident across various engineering domains, such as superplastic forming processes for bipolar plates [22] and wind tunnel simulations [23]. Additionally, analytical equations derived from FEA and ML algorithms provide accurate predictions for failure pressure in corroded pipelines [24] and the static behavior of bridge structures [25].

It should be noted that at least to the authors' knowledge, there have been no previous studies that integrate FEM simulation data with DL to generate images corresponding to physically consistent FEM simulation frames. This observation combined with the potential to replace FEM simulations for defect prediction with a more efficient DL network has inspired the current work.

III. Proposed Methodology

A. Overview

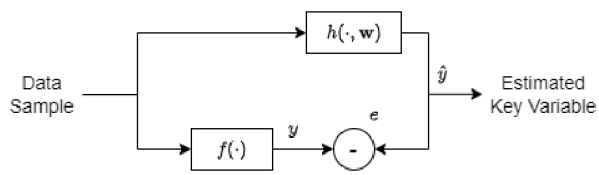

Fig. 2. Schematic overview of the proposed methodology. Before training, ANSYS^{TM} simulation software is used to extract ground truth simulation frames.

This framework translates the precision of FEM simulations into manufacturing predictions using a deep CNN. For each data sample $u(dx, dy, d\theta)$, representing antenna misplacement, two representations are generated, $I(u)$ from FEM simulations and $\hat{I}(u)$ from the CNN. The simulation frames $I(u)$ form a dataset $\{(u_i, I_i)\}_{i=1}^{N}$, which is used to train a network $h(u, \mathbf{w})$ such that

$$h(u, \mathbf{w}^*) \approx f(u) \tag{1}$$

where $f(\cdot)$ represents FEM and $\mathbf{w}^*$ are the optimal network parameters minimizing the cost function

$$\mathbf{w}^* = \arg\min_{\mathbf{w}} \sum_{i=1}^{N} L(h(u_i, \mathbf{w}), I_i)) \tag{2}$$

Here $L(h(u_i, \mathbf{w}), I_i)$ denotes a valid cost function. A schematic overview is provided in Fig. 2. The CNN predicts $h(u, w) = \hat{I}$, with its parameters adjusted to minimize the error $e = I - \hat{I}$.

B. Studied Use Case

This study focuses on the bending process in antenna manufacturing, where misplacement of the square tube at the antenna's core can cause defects such as wrinkling and fracturing. The square tube, designed with perforations to accommodate circular tubes, is bent using a blade as the upper forming tool to reduce wrinkling. Using CAD software and graphical data from the bending machine, a FEM model was developed to simulate bending-related phenomena, including deformation at stress-concentrated zones like perforations.

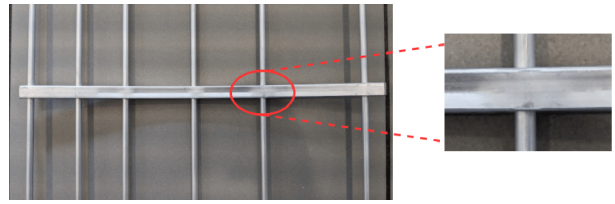

Fig. 3. Wrinkling of the aluminium profile.

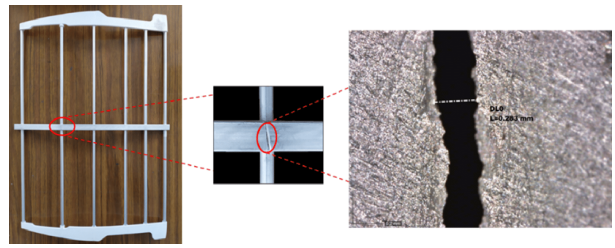

Fig. 4. Fracturing of the aluminium profile.

Defects like wrinkling and fracturing significantly impact production quality, as shown in Fig. 3 and 4, respectively. The studied defect types are the ones affecting production quality as identified by end-users. It is imperative to underscore the significance of the bending process in ensuring the quality of the produced antenna. Traditional FEM simulations occur offline, making real-time defect prevention challenging. This highlights the need for a predictive methodology that can estimate strain fields based on antenna misplacement during manufacturing, enabling timely defect mitigation and ensuring product quality.

C. FEM simulations

The ANSYS^{TM} software (Ansys® Academic Research Mechanical, Release 24.1, ANSYS, Inc., Canonsburg, PA, USA) was used to analyze the antenna's mechanical behavior during pneumatic press bending and to create a dataset for training a generative CNN for defect prediction. Explicit dynamic analysis captured the antenna's response to bending, modeling large deformations and bi-linear material behavior. Misalignment-induced strain was emphasized as a key factor in structural weaknesses.

Finite element analysis (FEA) simulated strain behavior and safety factors under various conditions, incorporating material properties derived from nanoindentation tests. A material erosion algorithm studied failure and separation, removing distorted elements along the aluminum beam based on fracture mechanics.

To replicate the bending process, velocity was applied to the bottom part while the blade was fixed, as shown in Fig. 5. The Courant-Friedrichs-Lewy (CFL) condition limited time-step size (0.001 s) for stability. Frictionless body interactions were assumed, and pre-existing defects were excluded. A conver-

This work is licensed under a Creative Commons Attribution-NonCommercial-NoDerivatives 4.0 License.
For more information, see https://creativecommons.org/licenses/by-nc-nd/4.0/

This article has been accepted for publication in IEEE Transactions on Instrumentation and Measurement. This is the author's version which has not been fully edited and content may change prior to final publication. Citation information: DOI 10.1109/TIM.2025.3568966

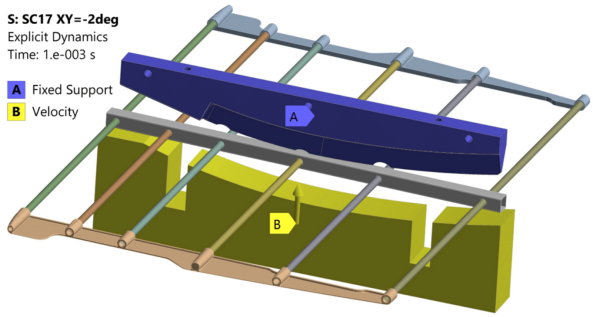

Fig. 5. Simulation setup showing the imposed velocity applied to the bottom part.

gence study validated mesh independence with approximately 262,100 elements, ensuring reliable stress predictions.

Using the ANSYS^{TM} software, 28 bending scenarios were simulated with FEM analysis, exploring x-axis and y-axis offsets (-3 to 3 mm) and rotations within the xy plane (-2 to 2 degrees). Each scenario produced 20 RGB frames (totalling 560 frames) showing strain evolution, with higher strain regions in red. The ANSYS^{TM} software generates 1628×580 pixel images, but most of the pixels contain irrelevant metadata. To focus on essential information, images were cropped to a 560×560 pixel area around the antenna body, which captures the critical strain data, as shown in Fig. 6. Finally, the frames were resized to 512×512 pixels for CNN compatibility.

To address the limited dataset size, spatial transformations including rotations ($\pm 5°$) and translations (± 2 mm) were applied to the input parameters and strain fields during training, simulating natural variations in antenna placement while preserving physical validity.

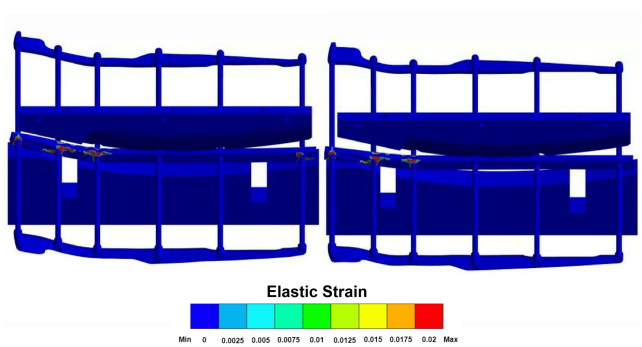

Fig. 6. Example of FEM simulation frames after preprocessing. Images are resized to 512 by 512 pixels after being cropped to focus on the relevant segments of the antenna configuration while removing unnecessary experimental references and backgrounds.

For dataset consistency, 80% of simulations (22) were used for training, and 20% (6) for validation and testing, preserving temporal and contextual integrity. A neural network was designed to input a vector of four parameters (x-axis, y-axis offsets, xy-plane rotation, and frame number) and output $512 \times 512 \times 3$ RGB images.

Preprocessing included writing metadata in CSV files, detailing filenames, translations, rotations, and frame numbers. This structured approach ensured efficient data handling, robust neural network training, and a strong foundation for further antenna manufacturing optimization.

The mesh convergence resulted in a predominance of hexahedral elements, ensuring higher numerical accuracy and computational efficiency. Tetrahedral elements were selectively used for the blade and HDPE plastic end parts, where complex geometries required finer meshing. The average element aspect ratio was 3.71, with a minimum value of 1.03, ensuring a well-shaped mesh for accurate stress distribution analysis. The FEA simulation was conducted on a system equipped with an AMD Ryzen 5 5600G processor (6 cores, 12 logical processors, 4.45 GHz) and 64 GB of RAM. The total computation time for the simulation was approximately 80 minutes under full CPU utilization.

D. Model Architecture

The framework uses a decoder with sequential residual upsampling blocks to transform a four-dimensional input (translation x, translation y, rotation xy, frame number) into a high-dimensional output, as seen in Fig. 7. Each block includes two transposed convolutional layers, two batch normalization layers, and a Rectified Linear Unit (ReLU). The model has 905,495 parameters, balancing accuracy and computational efficiency for strain field predictions.

The input tensor x is transformed into output tensor y with double the spatial dimensions using:

$$y = \Phi(x; \theta) + (x \uparrow 2) \tag{3}$$

where $(x \uparrow 2)$ denotes bicubic upsampling and θ represents learnable parameters. Residual connections improve learning from limited FEM data and mitigate overfitting.

The residual decoder consists of:

1) An initial linear layer for the latent vector (size 4).
2) A reshaping layer to convert the vector into a tensor.
3) Five residual upsampling blocks, transforming a $1024 \times 8 \times 8$ tensor into a $3 \times 512 \times 512$ image.

A convolutional autoencoder was implemented for image reconstruction tasks, consisting of a convolutional encoder and a convolutional residual decoder, as seen in Fig. 7. The encoder processes 3-channel inputs through four convolutional layers (4x4 filters, stride 2, padding 1), reducing filters from 96 to 12. Outputs are flattened into a $12 \times 32 \times 32$ vector, passed through a fully connected layer (64 units with ReLU), and mapped to 4 neurons using Sigmoid activation.

The residual decoder reconstructs images from a 1×4 latent vector, generating $1 \times 3 \times 512 \times 512$ outputs. Residual connections enhance image quality by easing gradient flow, retaining fine details, and reducing artifacts.

The autoencoder training involves two phases. First, the entire autoencoder (encoder and residual decoder) is trained end-to-end to minimize reconstruction loss, aligning output images with inputs and establishing a coherent mapping between image and latent spaces. In the second phase, only the residual decoder is fine-tuned using weights from the first phase. This initialization leverages prior learning, enhancing the decoder's ability to synthesize accurate and detailed images.

This work is licensed under a Creative Commons Attribution-NonCommercial-NoDerivatives 4.0 License.
For more information, see https://creativecommons.org/licenses/by-nc-nd/4.0/

This article has been accepted for publication in IEEE Transactions on Instrumentation and Measurement. This is the author's version which has not been fully edited and content may change prior to final publication. Citation information: DOI 10.1109/TIM.2025.3568966

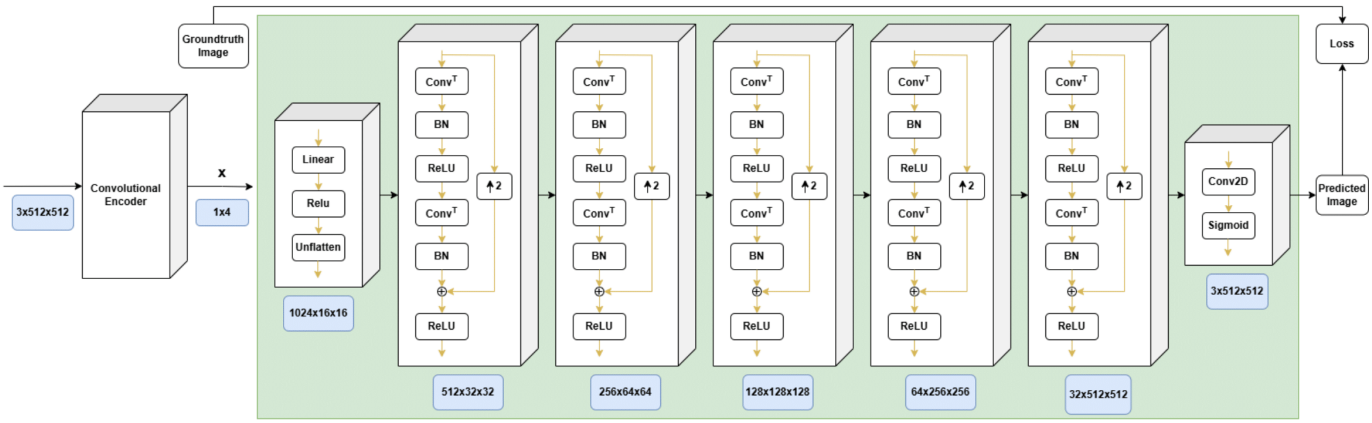

Fig. 7. Architecture of the residual decoder. The convolutional autoencoder consists of a convolutional encoder and a convolutional residual decoder. The latter one is enclosed in the the green border. The training process of the autoencoder consists of two phases, an initial training of the entire autoencoder in order to calculate and save the weights of the convolutional residual decoder and then a exclusive training of the residual decoder. The decoder is initialized with the weights obtained from the initial autoencoder training.

For benchmarking purposes, a simple convolutional decoder will also be trained and evaluated to compare its performance with the proposed residual decoder architecture. The same procedure, including prior training of a convolutional autoencoder, will be carried out to initialize the weights of the simple convolutional decoder.

To optimize the neural network's training for generating images from latent vectors, four loss functions were evaluated:: L_1, L_2, L_{VGG}, and L_C integrating both L_{VGG} and L_1.

L_1 (Mean Absolute Error) measures average absolute differences between predicted y_i and ground truth $\hat{y}_i$ values:

$$L_1 = \frac{1}{n}\sum_{i=1}^{n}|y_i - \hat{y}_i| \tag{4}$$

L_2 (Mean Squared Error) calculates average squared differences:

$$L_2 = \frac{1}{n}\sum_{i=1}^{n}(y_i - \hat{y}_i)^2 \tag{5}$$

The L_{VGG} uses pre-trained CNNs (e.g., VGG16, VGG19) to compute feature-wise differences between generated y and target $\hat{y}$ images based on feature map dissimilarity:

$$L_{VGG} = \frac{1}{n}\sum_{i=1}^{n} w_i \left\|\phi_i(y) - \phi_i(\hat{y})\right\|^2 \tag{6}$$

Here, ϕ_i represents the feature maps at layer i and w_i are layer weights. This loss emphasizes high-level perceptual similarity.

The L_C combines L_{VGG} and L_1:

$$L_C = a \times L_1 + b \times L_{VGG} \tag{7}$$

Coefficients a and b adjust the balance between pixel-level accuracy L_1 and perceptual similarity L_{VGG}. The weighting coefficients a and b were determined through comprehensive ablation studies, with results shown in Figure 9. Our experiments demonstrated that training convergence requires the L_1 weight a to be substantially smaller than the perceptual term weight b, with $a = 0.1$ representing the maximum stable value. The perceptual term (L_{VGG}) must dominate ($b \geq 0.6$) to generate physically plausible results, with optimal performance achieved at $a = 0.1$ and $b = 1.0$. This configuration ensures perceptual consistency while maintaining baseline pixel-level accuracy through minimal L_1 contribution.

The combined loss function, L_C, offers several advantages. By integrating L_1 for precise pixel-level accuracy and L_{VGG} for high-level perceptual similarity, L_C ensures the generated images are both realistic and detailed. This balanced approach improves the network's ability to retain structural details and fine textures while minimizing pixel-based discrepancies. Additionally, the flexibility of L_C allows adjustment of weighting coefficients to prioritize either perceptual or pixel accuracy, making it suitable for diverse application requirements. These benefits make L_C an optimal choice for generating wireframe bending images in antenna manufacturing.

E. Integration

Deployment follows a sequential quality control protocol, depicted in Figure 8. An industrial camera first captures the antenna position, while a computer vision system calculates misalignment parameters dx, dy and $d\theta$. These parameters are fed to an computing unit running the trained CNN model, which generates a complete strain simulation. The system then evaluates whether predicted strains exceed the manufacturer-defined threshold. For cases with excessive strain, it sends an actuation signal to remove and reposition the antenna. For acceptable strains, it authorizes the press controller via industrial protocols to initiate bending.

For reliable production deployment, the vision system incorporates vibration-resistant camera mounting, automated image quality checks, and calibration of exposure and focal length, along with regular lens maintenance and cleaning. Environmental hardening measures include protective housings and thermal stabilization of the installed camera. To enhance prediction robustness, the CNN is trained with synthetic noise augmentation. Additionally, mechanical guides are recommended to prevent extreme misplacements during antenna positioning.

This work is licensed under a Creative Commons Attribution-NonCommercial-NoDerivatives 4.0 License.
For more information, see https://creativecommons.org/licenses/by-nc-nd/4.0/

This article has been accepted for publication in IEEE Transactions on Instrumentation and Measurement. This is the author's version which has not been fully edited and content may change prior to final publication. Citation information: DOI 10.1109/TIM.2025.3568966

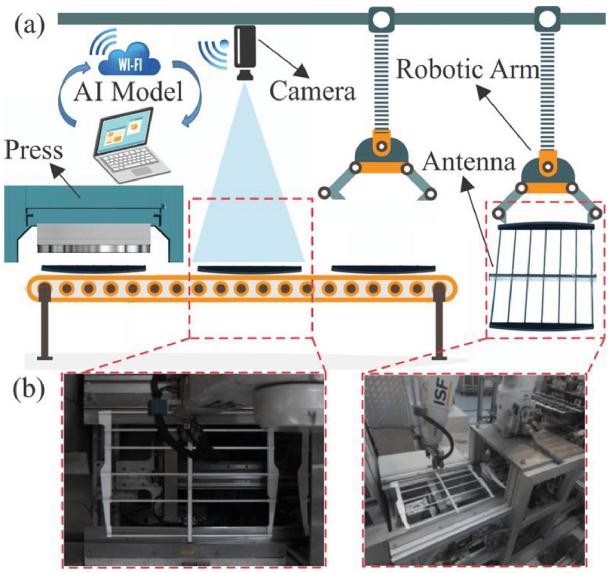

Fig. 8. Deployment of the proposed framework (a) System architecture showing vision system, the proposed trained CNN-based network, the press, and the actuation components (b) production floor deployment with camera, press controller, and robotic arm.

IV. Experimental Results and Analysis

A. Evaluation Metrics

To evaluate the neural network's performance in generating accurate antenna representations, three metrics were used: Mean Squared Error (MSE), Peak Signal-to-Noise Ratio (PSNR), and Structural Similarity Index (SSIM).

MSE quantifies pixel-level differences between the generated y and ground truth $\hat{y}$ images, where lower values indicate greater similarity. It is computed as follows:

$$MSE = \frac{1}{n \times m} \sum_{i=1}^{n} \sum_{j=1}^{m} (y_{i,j} - \hat{y}_{i,j})^2 \tag{8}$$

where n and m represent the height and width of the image, respectively. The terms $y_{i,j}$ and $\hat{y}_{i,j}$ denote the pixel intensity at position (i, j) in the generated and ground truth images, respectively. The summation calculates the squared differences between corresponding pixels, and the result is averaged over all pixels in the image to obtain the final MSE value.

PSNR measures reconstruction fidelity, with higher values indicating fewer perceptual errors. It is calculated as:

$$PSNR = 10 \times log(\frac{MAX^2}{MSE}) \tag{9}$$

where MAX represents the maximum possible pixel value (e.g., 255 for an 8-bit image).

SSIM evaluates structural similarity between images, considering luminance, contrast, and structure. SSIM produces a score ranging from -1 to 1, where 1 denotes perfect similarity between images:

$$SSIM(x, y) = \frac{(2\mu_x\mu_y + c_1)(2\sigma_{xy} + c_2)}{(\mu_x^2 + \mu_y^2 + c_1)(\sigma_x^2 + \sigma_y^2 + c_2)} \tag{10}$$

where μ_x represents the mean value of the image x, while μ_y represents the mean value of image y. The terms σ_x and σ_y refer to the standard deviations of images x and y, respectively, which measure the variability in pixel intensities. The term σ_{xy} represents the covariance between images x and y, indicating how the pixel values in the two images vary together. Finally, c_1 and c_2 are small constants used to stabilize the division with weak denominators, preventing division by zero.

B. Results

All of the experiments were conducted on the same environment, utilizing the NVIDIA GeForce RTX 3060 12GB as GPU, the Intel i5-12400F as CPU, 16 GB of RAM, and a Python 3.9 environment with Pytorch backend. During the training phase, each of the developed CNN models were trained until convergence. At the evaluation stage, a misplacement vector was provided and the trained model generated the image that visualizes the developed distribution fields over the antenna body during the bending process.

Figure 9 presents a quantitative analysis of the L_{VGG} weight (b) impact with fixed $a = 0.1$. All metrics show substantial improvement with increasing b values, with the optimal $b = 1.0$ configuration achieving 67% lower MSE (0.0022 vs 0.0067 at $b = 0.1$), 4.1 dB higher PSNR (26.84 dB vs 22.75 dB), and 18% greater SSIM (0.922 vs 0.873) compared to $b = 0.1$. While the overall trend shows monotonic improvement, deviations at $b = 0.4$ and $b = 0.9$ suggest complex interactions between the loss components. These results conclusively demonstrate that perceptual loss (L_{VGG}) is essential for predicting physically meaningful strain fields in our application.

Qualitative results for various misplacements are shown in Fig. 10. Each row represents a sample of a test misplacement, corresponding to $A = (-2, 3, -2)$, $B = (-2, -2, 0)$, $C = (-2, -1, -2)$, $D = (-2, 0, -2)$, respectively. Frames $\hat{I}_{10}$ and $\hat{I}_{20}$ are generated from the residual decoder, corresponding to the 10th and 20th frames, respectively, while I_{10} and I_{20} are the actual frames from the simulation at the same timestamps, computed by ANSYS™ software. For each CNN generated frame, the region of most interest is also highlighted, as this is where the most defects occur and the highest strain levels develop. Different strain levels are represented using a colormap, with higher strain levels indicated in red. The upper limit of 2% plastic strain is a practical criterion balancing safety, structural integrity, material performance, compliance with standards, and the long-term durability of the material. This limit helps ensure that aluminium alloys can perform reliably in their intended applications without experiencing detrimental permanent deformation. Notably, in all cases, the CNN generated 20th frame ($\hat{I}_{20}$), is visually close to the FEM calculated one (I_{20}).

To provide comprehensive architectural comparison, the Residual Decoder was benchmarked against three representative approaches: (1) a basic Convolutional Decoder as minimal baseline, (2) a Variational Auto Encoder (VAE) [26] decoder, and (3) a U-Net [27] decoder for its proven multi-scale capabilities in image synthesis. VAE and UNET decoders were

This work is licensed under a Creative Commons Attribution-NonCommercial-NoDerivatives 4.0 License.
For more information, see https://creativecommons.org/licenses/by-nc-nd/4.0/

This article has been accepted for publication in IEEE Transactions on Instrumentation and Measurement. This is the author's version which has not been fully edited and content may change prior to final publication. Citation information: DOI 10.1109/TIM.2025.3568966

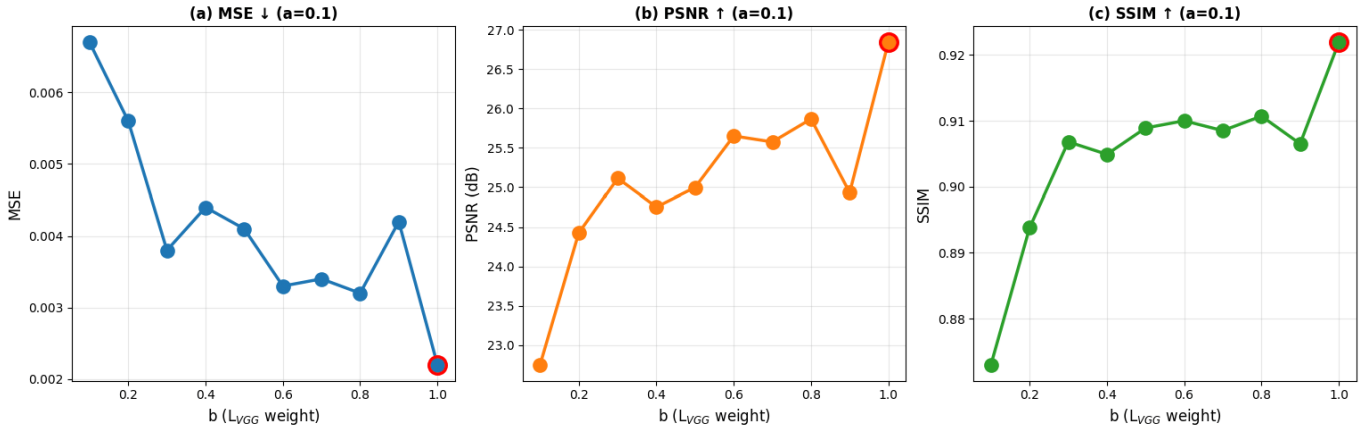

Fig. 9. Figure X: Impact of L_{VGG} weight (b) with fixed L_1 weight ($\alpha = 0.1$) on model performance. (a) MSE (lower values better), (b) PSNR (higher values better), and (c) SSIM (higher values better). Red circles mark the optimal configuration ($b = 1.0$).

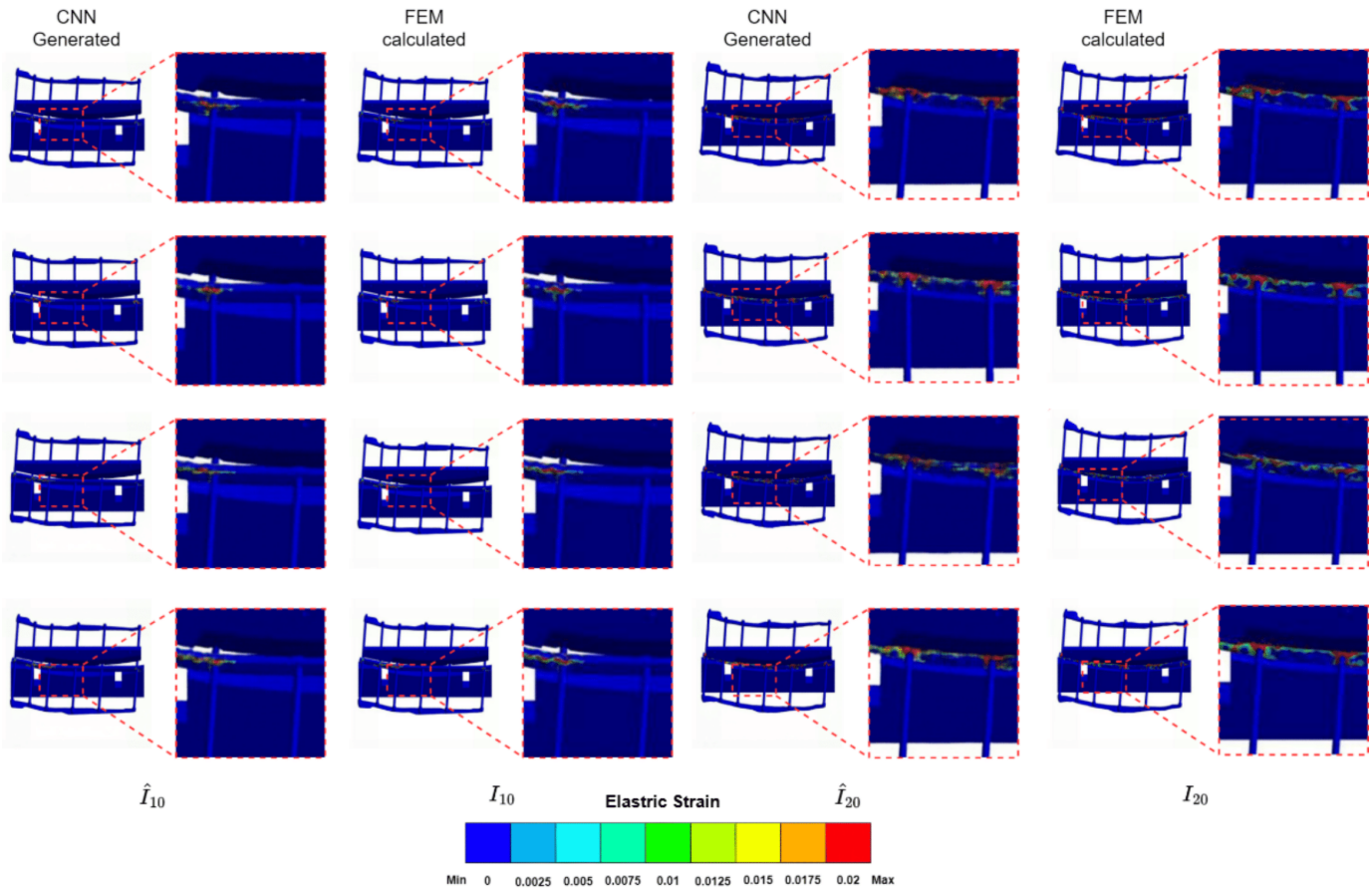

Fig. 10. Simulation results. Each of the total four rows, represents a misplacement in our test set. The misplacements correspond to $A = (-2, 3, -2)$, $B = (-2, -2, 0)$, $C = (-2, -1, -2)$, $D = (-2, 0, -2)$. The maximum strain that is developed in each one of cases is 0.93, 2.12, 1.88, 2.35, respectively. Next to each CNN generated frame, noted with $\hat{I}_i$, is depicted the FEM calculated frame I_i, produced by the ANSYS^{TM} software.

adapted to the specific task by removing skip connections and standardizing input/output dimensions. The experiments, summarized in Table I and Table II, reveal that the Residual Decoder achieves superior accuracy compared to all benchmarked architectures, including Convolutional, VAE, and U-Net decoders across all metrics (MSE, PSNR, and SSIM). The Residual Decoder with L_C loss achieves optimal performance (MSE=0.0022, PSNR=26.838, SSIM=0.9219), demonstrating both its accuracy and physical consistency. While the VAE decoder shows competitive results (MSE=0.0023, SSIM=0.9154) with 90% fewer parameters, and the U-Net variant achieves comparable SSIM (0.9117), the Residual Decoder maintains consistent advantages in prediction ability. Notably, the Convolutional Decoder's best configuration (L_2 loss) remains sub-

This work is licensed under a Creative Commons Attribution-NonCommercial-NoDerivatives 4.0 License.
For more information, see https://creativecommons.org/licenses/by-nc-nd/4.0/

This article has been accepted for publication in IEEE Transactions on Instrumentation and Measurement. This is the author's version which has not been fully edited and content may change prior to final publication. Citation information: DOI 10.1109/TIM.2025.3568966

TABLE I
NUMERIC RESULTS FOR THE DIFFERENT LOSS FUNCTIONS

Architecture	MSE ↓	PSNR ↑	SSIM ↑	Training Time ↓
Convolutional Decoder + L_1	0.0226	17.328	0.7954	48 min
Convolutional Decoder + L_2	0.0133	19.170	0.7913	50 min
Convolutional Decoder + L_{VGG}	0.0364	15.988	0.5471	95 min
Convolutional Decoder + L_C	0.0374	15.695	0.7687	73 min
Residual Decoder + L_1	0.0025	26.520	0.9163	34 min
Residual Decoder + L_2	0.0025	26.193	0.8948	24 min
Residual Decoder + L_{VGG}	0.0209	21.396	0.8634	80 min
Residual Decoder + L_C	**0.0022**	**26.838**	**0.9219**	69 min
VAE Decoder + L_1	0.0023	26.689	0.9154	69 min
VAE Decoder + L_2	0.0035	24.703	0.8900	22 min
VAE Decoder + L_{VGG}	0.0157	19.373	0.8961	62 min
VAE Decoder + L_C	0.0041	24.027	0.8573	60 min
UNET Decoder + L_1	0.0025	26.161	0.9131	34 min
UNET Decoder + L_2	0.0035	24.626	0.8912	**16 min**
UNET Decoder + L_{VGG}	0.0159	19.414	0.8385	41 min
UNET Decoder + L_C	0.0043	23.792	0.9117	29 min

TABLE II
NUMBER OF PARAMETERS FOR THE DIFFERENT ARCHITECTURES

Architecture	Parameters
Convolutional Decoder	905,495
Residual Decoder	11,441,123
VAE Decoder	1,029,299
UNET Decoder	12,488,451

stantially inferior (MSE=0.0133, PSNR=19.170), highlighting the importance of residual connections for this task.

The choice of loss function plays a crucial role in model performance, with optimal selections varying significantly by architecture. For the Convolutional Decoder, L_2 and L_1 losses yield better results (MSE=0.0133 and 0.0226 respectively), while L_{VGG} and L_C underperform (MSE>0.036). The VAE decoder shows different preferences, achieving best results with L_1 (MSE=0.0023), whereas the U-Net performs optimally with L_1 and L_C (MSE=0.0025 and 0.0043). In contrast, the Residual Decoder demonstrates robust performance across all loss functions, with L_C yielding the overall best metrics (MSE=0.0022, SSIM=0.9219). These findings highlight that while loss function sensitivity is architecture-dependent, the Residual Decoder provides both superior performance and greater training stability across loss variants.

The training times, depicted in Table I, range from 16 minutes (UNET Decoder + L_2) to 95 minutes (Convolutional Decoder + L_{VGG}), with the optimal configuration (Residual Decoder + L_C) requiring 69 minutes. While these training times are comparable to a single FEM simulation ($\sim$80 minutes), FEM incurs significant hidden costs: each simulation requires hours of expert-led setup (e.g., mesh generation, boundary condition configuration, and material property calibration) and must be rerun for every new scenario. By contrast, the proposed network incurs a one-time training cost and subsequently generates predictions in seconds per simulation without requiring FEM expertise.

V. CONCLUSION

This study presents an innovative approach to defect prediction in antenna manufacturing by integrating Finite Element Method (FEM) simulations with deep learning (DL) techniques. Through the use of generative convolutional neural networks (CNNs), the proposed framework efficiently generates physically consistent strain distributions, addressing the high computational cost of traditional FEM simulations. The experimental results demonstrate the effectiveness of the model in predicting defects during antenna bending, with performance metrics that closely match FEM-calculated outcomes, but with significantly faster inference times. This advancement not only offers practical advantages for real-time defect prediction but also supports the optimization of manufacturing processes, ultimately improving production efficiency and product quality.

Despite the promising results, the methodology faces certain limitations, including the need for further fine-tuning to improve robustness and extend its application to a broader range of manufacturing scenarios. Future work could explore the optimization of the proposed model, incorporating more diverse manufacturing processes and enhancing its scalability. Moreover, expanding the integration of CNN-based deep learning-driven predictions with real-time control systems could further enhance the overall defect prevention strategy across various industries. As manufacturing processes continue to evolve, this work paves the way for deeper integration of CNN-based deep learning with simulation-based methodologies, ensuring smarter and more efficient production lines.

REFERENCES

[1] W. He, Z. Jiang, W. Ming, G. Zhang, J, Yuan and L Yin. "A critical review for machining positioning based on computer vision," *Measurement*, vol. 84, pp. 109973, 2021.

[2] D.G. Lema, O.D. Pedrayes, R. Usamentiaga, P. Venegas and D.F. García. "Automated detection of subsurface defects using active thermography and deep learning object detectors," *IEEE Transactions on Instrumentation and Measurement*, vol. 71, pp. 1–13, 2022.

[3] Y. Cao, Y. Ni, Y. Zhou, H. Li, Z. Huang and E. Yao. "An Auto Chip Package Surface Defect Detection Based on Deep Learning," *IEEE Transactions on Instrumentation and Measurement*, 2023.

[4] T. Sui and J. Wang. "DMPDD-Net: An Effective Defect Detection Method for Aluminum Profiles Surface Defect," *IEEE Transactions on Instrumentation and Measurement*, 2024.

[5] S. She, X. Zheng, L. Xiong, T. Meng, Z. Zhang, Y. Shao, W. Yin, J. Shen and Y. He. "Thickness Measurement and Surface-defect Detection for Metal Plate Using Pulsed Eddy Current Testing and Optimized Res2Net Network," *IEEE Transactions on Instrumentation and Measurement*, 2024.

[6] X. Zhang, Z. Long, J. Peng, G. Wu, H. Hu, M. C. Lyu, G. Qin and D. Song. "Fault prediction for electromechanical equipment based on spatial-temporal graph information," *IEEE Transactions on Industrial Informatics*, vol. 19, no. 2, pp. 1413–1424, 2022.

[7] Y. Jia, L. Ying, D. Wang, and J. Zhang. "Defect prediction of relay protection systems based on LSSVM-BNDT," *IEEE Transactions on Industrial Informatics*, vol. 17, no. 1, pp. 710–719, 2020.

[8] O. C. Zienkiewicz, R. L. Taylor, and J. Z. Zhu. *The finite element method: its basis and fundamentals*, Elsevier, 2005.

[9] R. Rai, M. K. Tiwari, D. Ivanov, and A. Dolgui. "Machine learning in manufacturing and industry 4.0 applications," *International Journal of Production Research*, vol. 59, no. 16. Taylor & Francis, pp. 4773–4778, 2021.

[10] S. Shahrabadi, Y. Castilla, M. Guevara, L. G. Magalhães, D. Gonzalez, and T. Adão. "Defect detection in the textile industry using image-based machine learning methods: a brief review," *Journal of Physics: Conference Series*, 2022, vol. 2224, p. 012010.

[11] A. Saberironaghi, J. Ren, and M. El-Gindy. "Defect detection methods for industrial products using deep learning techniques: a review," *Algorithms*, vol. 16, no. 2, p. 95, 2023.

This work is licensed under a Creative Commons Attribution-NonCommercial-NoDerivatives 4.0 License.
For more information, see https://creativecommons.org/licenses/by-nc-nd/4.0/

This article has been accepted for publication in IEEE Transactions on Instrumentation and Measurement. This is the author's version which has not been fully edited and content may change prior to final publication. Citation information: DOI 10.1109/TIM.2025.3568966

[12] L. Leontaris, A. Mitsiaki, P. Charalampous, N. Dimitriou, E. Leivaditou, A. Karamanidis, G. Margetis, . "A blockchain-enabled deep residual architecture for accountable, in-situ quality control in industry 4.0 with minimal latency," *Computers in Industry*, vol. 149, p. 103919, 2023.

[13] S. Jain, G. Seth, A. Paruthi, U. Soni, and G. Kumar. "Synthetic data augmentation for surface defect detection and classification using deep learning," *Journal of Intelligent Manufacturing*, pp. 1–14, 2022.

[14] G. Zhang, K. Cui, T.-Y. Hung, and S. Lu. "Defect-GAN: High-fidelity defect synthesis for automated defect inspection," in *Proceedings of the IEEE/CVF Winter Conference on Applications of Computer Vision*, 2021, pp. 2524–2534.

[15] N. Dimitriou, L. Leontaris, T. Vafeiadis, D. Ioannidis, T. Wotherspoon, G. Tinker and D. Tzovaras. "A deep learning framework for simulation and defect prediction applied in microelectronics," *Simulation Modelling Practice and Theory*, vol. 100, p. 102063, 2020.

[16] E. Oñate, A. Franci, and J. M. Carbonell. "A particle finite element method for analysis of industrial forming processes," *Computational Mechanics*, vol. 54, pp. 85–107, 2014.

[17] B. V. Golechha and P. S. Kulkarni. "Design, analysis and optimization of 10 ton pneumatic press machine," *International Journal of Advanced Research in science, Engineering and Technology*, vol. 4, no. 3, 2017.

[18] A. Shirdel, A. Khajeh, and M. M. Moshksar. "Experimental and finite element investigation of semi-constrained groove pressing process," *Materials & Design*, vol. 31, no. 2, pp. 946–950, 2010.

[19] M. S. Joun and M. C. Lee. "Quadrilateral finite-element generation and mesh quality control for metal forming simulation," *International Journal for Numerical Methods in Engineering*, vol. 40, no. 21, pp. 4059–4075, 1997.

[20] X. Liu, M. Xia, D. Bolati, J. Liu, Q. Zheng, and H. Zhang. "An ANN-based failure pressure prediction method for buried high-strength pipes with stray current corrosion defect," *Energy Science & Engineering*, vol. 8, no. 1, pp. 248–259, 2020.

[21] L. von Rueden, S. Mayer, R. Sifa, C. Bauckhage, and J. Garcke. "Combining machine learning and simulation to a hybrid modelling approach: Current and future directions," in *Advances in Intelligent Data Analysis XVIII: 18th International Symposium on Intelligent Data Analysis, IDA 2020, Konstanz, Germany, April 27–29, 2020, Proceedings 18*, 2020, pp. 548–560.

[22] I. Choirotin and M. A. Choiron. "Defect Prediction at the Superplastic Forming Process of the Bipolar Plate by Simulation," *Journal of Energy, Mechanical, Material, and Manufacturing Engineering*, vol. 3, no. 1, pp. 49–54, 2018.

[23] L. A. Al-Haddad, A. A. Jaber, L. Ibraheem, S. A. Al-Haddad, N. S. Ibrahim, and F. M. Abdulwahed. "Enhancing wind tunnel computational simulations of finite element analysis using machine learning-based algorithms," *Eng Technol J*, vol. 42, no. 1, pp. 1–9, 2023.

[24] S. D. Vijaya Kumar, S. Karuppanan, and M. Ovinis. "Failure pressure prediction of high toughness pipeline with a single corrosion defect subjected to combined loadings using artificial neural network (ANN)," *Metals*, vol. 11, no. 2, p. 373, 2021.

[25] Y. Wu, L. Zhang, H. Liu, and P. Lu. "Stress prediction of bridges using ANSYS soft and general regression neural network," in *Structures*, 2022, vol. 40, pp. 812–823.

[26] X. J. Mao, C. Shen and Y. B. Yang. "Image restoration using convolutional auto-encoders with symmetric skip connections," in *arXiv preprint arXiv:1606.08921*, 2016.

[27] O. Ronneberger, P. Fischer and T. Brox. "U-net: Convolutional networks for biomedical image segmentation," in *Medical image computing and computer-assisted intervention–MICCAI 2015: 18th international conference, Munich, Germany, October 5-9, 2015, proceedings, part III 18*, 2015, pp. 234–241.

Anastasios Tzelepakis received the diploma in electrical and computer engineering from the Democritus University of Thrace, Xanthi, Greece, in 2021.

He has been a Research Assistant with the Information Technologies Institute, Centre for Research and Technology Hellas, Thessaloniki, since October 2022. His research interests include deep learning, computer vision and generative artificial intelligence.

Nikolaos Dimitriou (Member, IEEE) received his Diploma and Ph.D. degrees in Electrical and Computer Engineering from the Aristotle University of Thessaloniki, Greece, in 2007 and 2014, respectively.

He is currently a Senior Researcher (Grade C') at the Information Technologies Institute, Centre for Research and Technology Hellas (CERTH), Thessaloniki, Greece. His research interests include computer vision and deep learning, with a particular focus on industrial applications.

Paschalis Charalampous received the Diploma degree in mechanical engineering, master's degree in processes & advanced materials technologies, and Ph.D. degree in manufacturing procedures from the Mechanical Engineering Department, Aristotle University of Thessaloniki, Thessaloniki, Greece, in 2013, 2015, and 2018, respectively.

He has academic teaching experience with the Department of Mechanical Engineering in Aristotle University of Thessaloniki, as well as in the International Hellenic University, Thermi, Greece. He has authored or coauthored more than 30 papers in international scientific journals and more than 20 papers in international conferences. His research interests include manufacturing engineering, material science, mechanical engineering design, and additive manufacturing procedures.

Konstantinos Tsongas received the Diploma degree in Civil Engineering, the Master's degree in Advanced Materials, and the Ph.D. degree in Mechanical Engineering from Aristotle University of Thessaloniki, specializing in composite materials and optimization tools for mechanical systems.

Currently, he is an Assistant Professor in the Industrial Engineering and Management Department of the International Hellenic University (I.H.U.), Greece. His research interests include additive manufacturing of nanocomposite and recycled polymers, lattice structures, material characterization, dynamic mechanical analysis, digital twins, finite element analysis, and optimization processes.

Dimitrios Tzetzis received his Ph.D. from Queen Mary, University of London, School of Engineering and Materials Science, where he was a member of the Centre for Materials Research.

Curerntly, he is an Associate Professor and Head of the Digital Manufacturing and Materials Characterization Laboratory and Director of the MSc in Strategic Product Design at the International Hellenic University, Greece. He also serves as a visiting professor and researcher at various educational institutions in Greece and abroad. His research interests include 3D digital technologies, additive manufacturing, mechanical analysis of structures, and the development and assessment of advanced materials.

This work is licensed under a Creative Commons Attribution-NonCommercial-NoDerivatives 4.0 License.
For more information, see https://creativecommons.org/licenses/by-nc-nd/4.0/

This article has been accepted for publication in IEEE Transactions on Instrumentation and Measurement. This is the author's version which has not been fully edited and content may change prior to final publication. Citation information: DOI 10.1109/TIM.2025.3568966

Dimitrios Tzovaras (Senior Member, IEEE) received the Diploma and the Ph.D. degree in electrical and computer engineering from Aristotle University of Thessaloniki, Thessaloniki, Greece, in 1992 and 1997, respectively.

He is the Director at the Information Technologies Institute of the Centre for Research and Technology Hellas. His main research interests include visual analytics, 3D object recognition, search and retrieval, behavioral biometrics, assistive technologies, information and knowledge management, computer graphics, and virtual reality.

This work is licensed under a Creative Commons Attribution-NonCommercial-NoDerivatives 4.0 License.
For more information, see https://creativecommons.org/licenses/by-nc-nd/4.0/